Materials Science & Engineering A 582 (2013) 235–244

Contents lists available at SciVerse ScienceDirect

Materials Science & Engineering A

journal homepage: www.elsevier.com/locate/msea

Bulk combinatorial design of ductile martensitic stainless steels through confined martensite-to-austenite reversion

H. Springer *, M. Belde, D. Raabe

Max-Planck-Institut für Eisenforschung GmbH, 40237 Düsseldorf, Germany

ARTICLE INFO

Article history:
Received 21 March 2013
Received in revised form
5 June 2013
Accepted 8 June 2013
Available online 20 June 2013

Keywords:
Steels
Mechanical properties
Microstructure
Transformation induced plasticity
Combinatorial alloy design

ABSTRACT

The effect of local martensite-to-austenite reversion on microstructure and mechanical properties was studied with the aim of designing ductile martensitic steels. Following a combinatorial screening with tensile and hardness testing on a matrix of six alloys (0–5 wt% Mn, 0–2 wt% Si, constant 13.5 wt% Cr and 0.45 wt% C) and seven martensite tempering conditions (300–500 °C, 0–30 min), investigations were focussed on martensite-to-austenite reversion during tempering as function of chemical composition and its correlation with the mechanical properties. While Mn additions promoted austenite formation (up to 35 vol%) leading to a martensitic–austenitic TRIP steel with optimum mechanical properties (1.5 GPa ultimate tensile strength and 18% elongation), Si led to brittle behaviour despite even larger austenite contents. Combined additions of Mn and Si broadened the temperature range of austenite reversion, but also significantly lowered hardness and yield strength at limited ductility. These drastically diverging mechanical properties of the probed steels are discussed in light of microstructure morphology, dispersion and transformation kinetics of the austenite, as a result of the composition effects on austenite retention and reversion.

1. Introduction

Steels are the most versatile structural materials owing to their multiple equilibrium and non-equilibrium phase transformations. These enable a huge variety of easy to manipulate kinetic pathways that lead to an unprecedented spectrum of mechanical properties through the intrinsic nano-structuring of the bulk materials. Examples are soft interstitial free steels with less than 200 MPa flow stress and more than 60% elongation [1], twinning induced plasticity (TWIP) steels offering superior ductility above 70% elongation [2–5], weight reduced "Triplex" steels with up to 1.5 GPa strength and yet more than 40% elongation [6–10], or pearlitic wires that can be drawn to a strength beyond 6 GPa, stronger than any other bulk material [11–13]. On the other hand, steels – like all other structural materials – suffer from the fact that an increase in strength via traditional hardening mechanisms is associated with a decrease in ductility. This inverse stress–strain relationship is currently the strongest limitation to the further development of advanced alloys. It limits particularly the application of carbon-based (C) martensite, the strongest single phase attainable in steel, despite its very high potential for enabling a cost-efficient novel generation of ductile high strength steels.

In order to overcome this inverse relationship between strength and ductility, the hard and strong martensitic matrix can be blended e.g. with ductile ferrite as in dual-phase steel microstructures [14,15] or with instable and compliant austenite. Utilisation of the latter approach offers the additional advantage that when exposed to mechanical load, it can back-transform to martensite, acting as additional strain hardening effect through the transformation induced plasticity (TRIP) mechanism [16–19]. The austenite may be incorporated as a retained (i.e. present in the as-quenched state) and/or reverted phase (formed and stabilised during subsequent tempering) [20–26], and designed close or even beyond its mechanical or thermodynamic stability limit [27–31]. Stabilisation of austenite for retention after cooling to room temperature may be achieved by substitutional alloying, e.g. with nickel (Ni) or manganese (Mn). Interstitial austenite formers such as nitrogen (N) or C can furthermore be readily partitioned during intercritical annealing [32], or, following a more recent approach, after quenching just below martensite start temperature M_S and immediate tempering [33,34].

Reverted austenite typically offers greater microstructural synergy with martensite than retained austenite, as it creates thin, compliant interlayers at the martensite grain boundaries upon reversion treatment [22,23,35–37]. These layers have been shown to form a sort of composite structure, inhibiting crack propagation otherwise prevalent along the {100} planes of the martensite laths, and have thus been linked to increased toughness and decreased ductile–brittle transition temperatures [37,38]. By choosing appropriate chemical compositions and thermo-mechanical treatments (TMT), the austenite formed via

* Corresponding author. Tel.: +49 211 6792 796; fax: +49 211 6792 333.
E-mail address: h.springer@mpie.de (H. Springer).

0921-5093/$ - see front matter © 2013 Elsevier B.V. All rights reserved.
http://dx.doi.org/10.1016/j.msea.2013.06.036

reversion can be adjusted in terms of volume fraction, dispersion and morphology in order to tailor the properties of the microstructure by self-organization via grain-scale diffusion, grain boundary segregation and selective phase transformation [22,23,31,35].

These advantageous effects of reverted austenite incorporated within a martensitic matrix have thus prompted exploitation in works on various steel designs such as supermartensitic steels [31,39,40], austenitic [24,26] and martensitic stainless steels [28–30,35]; mainly focussing on reversion kinetics, influence of heating rate, martensite history and texture memory/orientation relationships. Yuan et al. [35] studied the mechanisms governing the austenite reversion with atom probe tomography (APT) measurements of a martensitic stainless steel (1.4034, 13.5 wt% chromium (Cr), 0.44 wt% C). They found that during tempering at 400 °C subsequent to quenching from 1150 °C, C rapidly left the martensite and segregated at lattice defects as well as in retained austenite grains ('kinetic freezing', by the combination of high C solubility but low diffusivity). By tailoring the nano-scaled austenite with respect to content and size, ultra-high strength of up to 2 GPa was achieved while maintaining good ductility (about 20% tensile elongation) [35].

In light of these numerous investigations regarding the favourable impact of reversed-austenite regions on the mechanical properties of high strength martensitic steels, it is of interest to systematically study the influence of alloying elements. Of special relevance are Mn and silicon (Si), as they are not only common accompanying elements in commercially available Cr–C alloyed steels, but also expected to exert strong effects while being cost effective [41–47]. Despite ongoing developments in theoretical thermodynamics calculation methods [48,49], however, the related microstructural phenomena which determine the mechanical properties of such steels are far from equilibrium and thus still difficult to comprehensively predict. This is further complicated by the large possible variety of chemical compositions in the Fe–Cr–C–Si/Mn systems and, accordingly, large possible variations in associated TMT setups (e.g. tempering time and temperature). As an experimental alternative, combinatorial techniques can effectively probe optimal synthesis and processing cycles of a multitude of chemical concentrations [50,51] and microstructural variations [52,53]. The recently introduced RAP approach, which is based on semi-continuous high-throughput bulk casting, rolling, heat treatment and sample preparation techniques, has demonstrated its effectiveness in performing an accelerated screening of the tensile, hardness and microstructural properties as a function of chemical and TMT parameters both systematically and efficiently [6]. It thus enables to effectively identify compositional and microstructural trends that are relevant for the bulk mechanical behaviour of the investigated steels.

2. Objective

The specific objective of this work is to systematically study the influence of additions of Mn and Si on the microstructure and mechanical properties of 13.5Cr–0.45C (wt%) based steels dependent on tempering time and temperature. The focus of this combinatorial study of the compositional and thermo-mechanical variations lies in identifying ideal conditions for the interface reversion mechanism and austenite stability with respect to enhancing martensite ductility.

3. Materials and methods

3.1. Combinatorial sample synthesis procedure

Six Fe–13.5Cr–0.45C based alloys with different additions of Mn, Si as well as both Mn and Si combined (Table 1) were produced and processed by multiple runs of the RAP method detailed elsewhere [6]. After melting in a vacuum induction furnace and casting into copper moulds, 80% thickness reduction was achieved by rolling the ingots at 1000 °C to 2 mm thick stripes, followed by air cooling to room temperature. Homogenisation was conducted by annealing at 1150 °C for 1 h under argon atmosphere and water quenching. Tempering was performed at 300, 400 and 500 °C for 0, 10 and 30 min each (in air, oil quenching to room temperature) for all investigated alloy compositions (0 min representing the as-quenched state). The different alloys are referred to by their target alloy composition in wt% (Table 1) throughout this work.

Table 1
Target and actual chemical composition in wt% of the investigated alloys.

Target values (wt%)	Actual values (wt%)
Fe–13.5Cr–0.45C	Fe–13.4Cr–0.46C
Fe–13.5Cr–0.45C–2.5Mn	Fe–13.3Cr–0.45C–2.57Mn
Fe–13.5Cr–0.45C–5Mn	Fe–12.8Cr–0.41C–5.03Mn
Fe–13.5Cr–0.45C–1Si	Fe–13.8Cr–0.47C–1.08Si
Fe–13.5Cr–0.45C–2Si	Fe–13.4Cr–0.46C–2.08Si
Fe–13.5Cr–0.45C–2.5Mn–2Si	Fe–13.3Cr–0.48C–2.44Mn–2.05Si

3.2. Mechanical testing and characterisation

After preparing flat sheet tensile specimens (17.89 mm gauge length) by spark erosion, testing was conducted at room temperature with an initial strain rate of 10^{-3} s^{-1} using a hydraulic testing machine Instron 8511. Macro-hardness (Rockwell C) was measured with a Wolpert DIA Testor 2RC on the outer surface (rolling plane) of the segments after grinding them to 1000 grit. All values of both tensile and macro-hardness testing represent average data of three measurements for every alloy/tempering combination.

Cross sectional areas of the specimens were prepared in the plane perpendicular to the rolling direction by grinding and polishing with standard metallographic techniques. The cross sections were investigated via optical microscopy (OM; Zeiss Axiophot 1) and scanning electron microscopy (SEM; Jeol JSM 6490). Phase identification was performed via electron backscatter diffraction analysis (EBSD; EDAX OIM software v.6.2.0), using representative mappings of about 0.2 mm^2 and a step size of 1 μm. Nano-indentation was carried out on the OM and SEM observation plane, using a Hysitron TriboIndenter equipped with a Ti 39-1 Bercovich tip at a constant load of 1000 μN with a step size of 4 μm.

4. Results

The mechanical data of the six alloys (Table 1) in their various tempering conditions are plotted as an overview in Fig. 1. Yield strength (YS; Fig. 1a), ultimate tensile strength (UTS; Fig. 1b), total elongation (TE; Fig. 1c) and macro-hardness (Fig. 1d) are shown as function of alloying additions to the 13.5Cr–0.45C (wt%) based steels and colour-coded corresponding to the respective tempering treatments. The reference material without any alloying additions, i.e. Fe–13.5Cr–0.45C, exhibits its highest hardness in the as-quenched state (~52 HRC) and, as expected, corresponding brittle behaviour during tensile testing (premature failure at low strains despite high inherent strength). Upon tempering the reference alloy becomes more ductile – increasing with temperature – with a maximum TE value of about 15% after tempering at 500 °C for 10 min. This increase in ductility allows for better utilising the materials strength, which results in higher UTS values after tempering, despite lower respective hardness values than in the as-quenched state. The same tendency applies for the YS

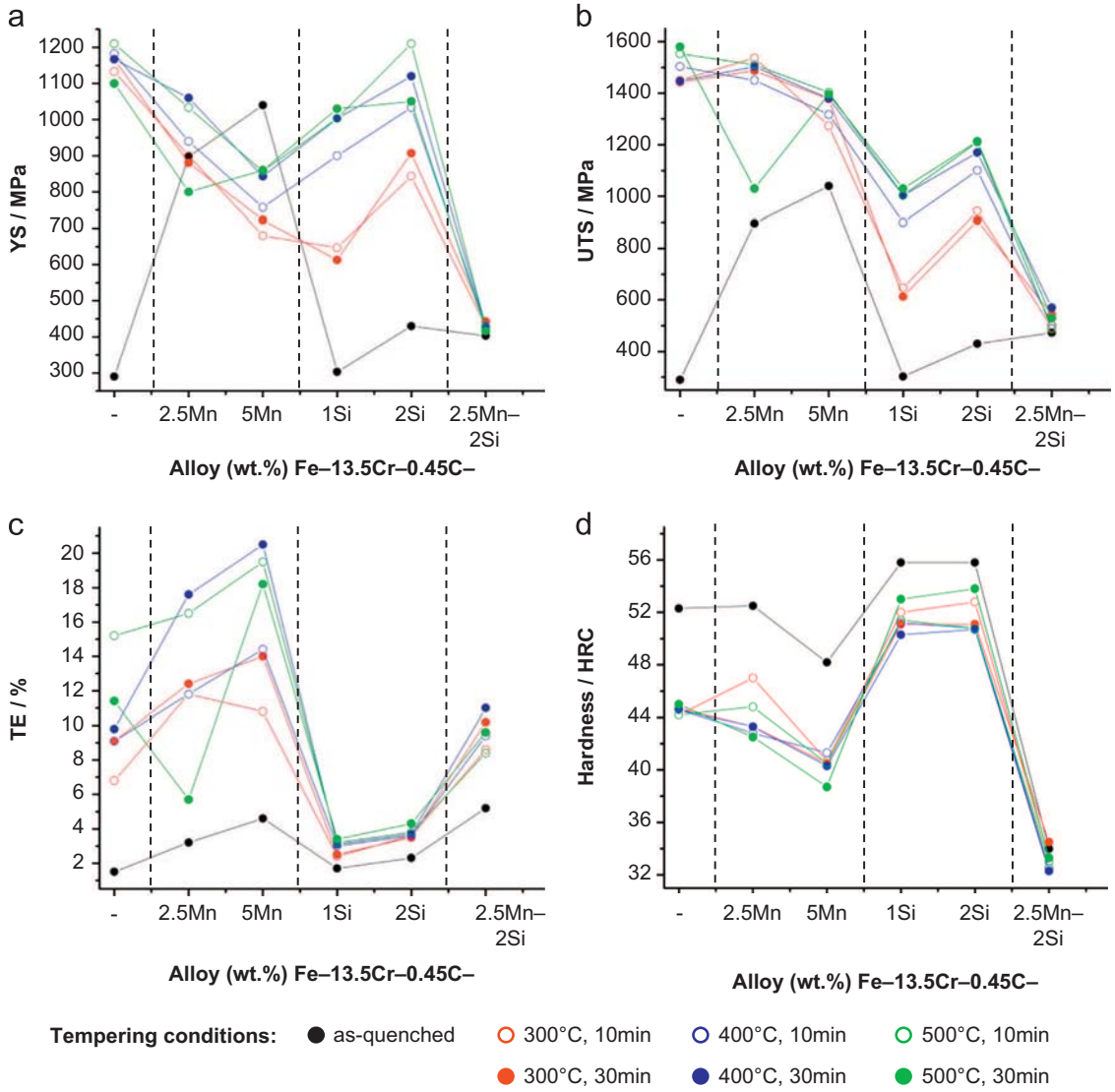

Fig. 1. Overview of the mechanical properties as a function of chemical composition (Table 1) and the applied tempering treatments: (a) yield stress (YS); (b) ultimate tensile stress (UTS); (c) total elongation (TE); (d) macro-hardness.

(1.1–1.2 GPa) and UTS (1.4–1.6 GPa), while the macro-hardness of Fe–13.5Cr–0.45C remains constant during tempering at about 45 HRC. Adding Mn gradually reduces the brittleness in the as-quenched state with increasing Mn concentrations. After tempering, the Mn alloyed steels have lower YS, UTS and macro-hardness values than the respective reference material conditions (decreasing with Mn content), while the ductility is increased to up to 21% for the Fe–13.5Cr–0.45C–5Mn material. The highest respective values of YS, UTS and TE are observed for tempering the Mn alloyed materials at 400 °C for 30 min. Additions of 1 and 2 wt% Si result in the highest macro-hardness of all the alloys studied in this work (56 HRC in the as-quenched state), which is slightly reduced to values between 50 and 54 HRC by tempering. YS and UTS increase with the tempering temperature. The ductility, on the other hand, is with TE values between 2% and 4% lower than for all the other investigated alloys and no necking of the Si alloyed samples could be observed. Opposed to the aforementioned trends observed when alloying with Mn (increase in ductility and drop in strength) and Si (increase in hardness and higher embrittlement), the simultaneous addition of Mn and Si leads to a drastically different mechanical behaviour: Almost independent of the tempering conditions, the Fe–13.5Cr–0.45C–2.5Mn–2Si material is softer (31–35 HRC) and has both, lower YS (400–450 MPa) and UTS (480–600 MPa) when compared to the other alloys studied here. The ductility of the Mn–Si alloyed steel is about 4% in the as-quenched state, and it increases more strongly upon tempering than that of the Si alloyed steels. However, despite the materials' comparatively low strength the ductility remains far below the respective values reached by solely Mn alloyed materials with a maximum TE of only 11%.

The above mentioned trends in terms of chemistry-related mechanical properties are illustrated in Fig. 2a by four selected tensile curves after tempering at 400 °C for 30 min. In spite of the drastically differing tensile testing behaviour of the four alloys, corresponding SEM fractography analysis (Fig. 2b–e) revealed inter- and trans-granular cleavage as the dominant failure mechanism of all samples, with small ridges resembling ductile failure (highlighted by white arrows in Fig. 2b–e). No clear microstructural evidence linked to the varying mechanical data could be observed in the fractured surfaces. The low apparent elastic moduli of the alloys are an artefact of the applied high throughput testing procedure

OM and SEM investigations (Fig. 3) revealed a predominantly martensitic microstructure for the samples in the as-quenched

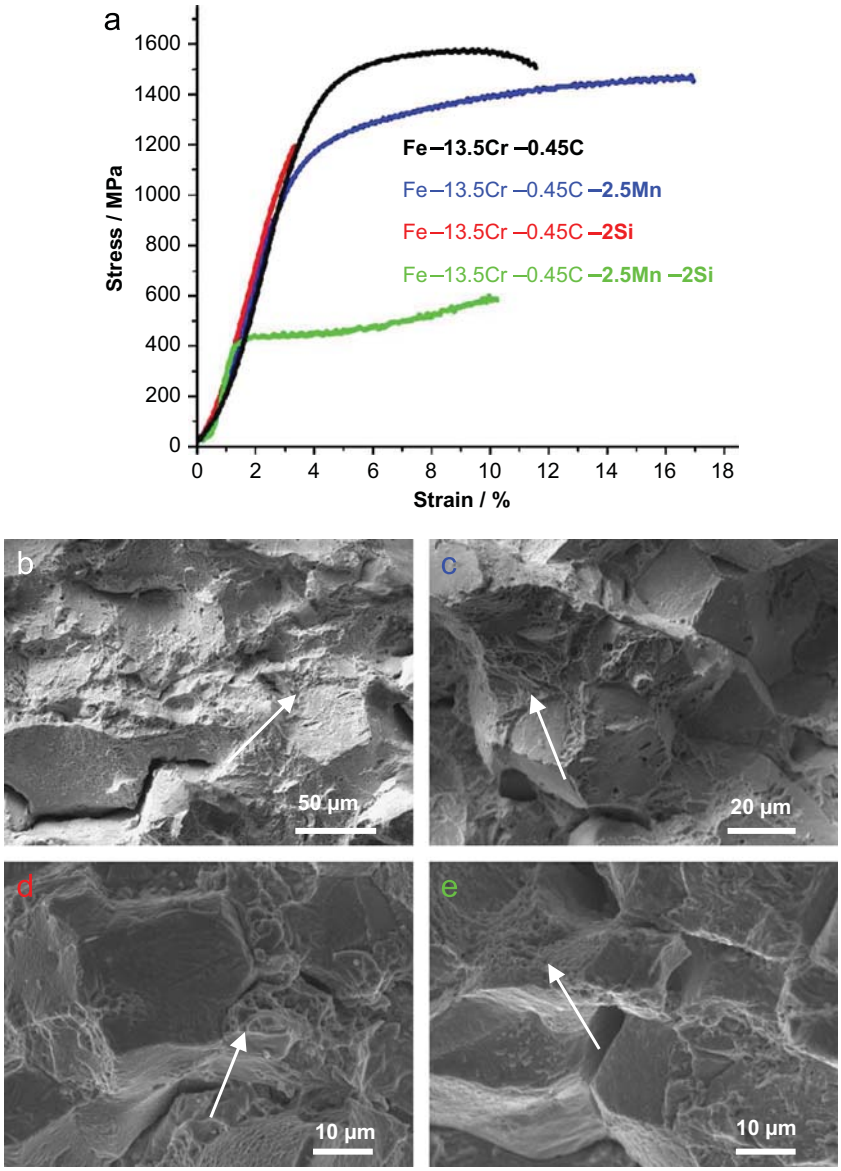

Fig. 2. (a) Exemplary engineering stress/strain curves from selected alloys after tempering at 400 °C for 30 min; (b–e) corresponding SEM fractographs.

state (former austenite grain size roughly about 100 µm; Fig. 3a), along with few coarse carbides of about 1 µm diameter (most probably non-dissolved primary carbides; Fig. 3b). In the tempered state, varying amounts of finely dispersed nano-scaled carbide platelets were observed, most notably in the Si-free samples. Aside from these observations, no pronounced variations between the different alloys were found except for the amount of austenite, which was also observed to change drastically with tempering conditions. The temperature dependence (tempering time 30 min) of the austenite fraction is shown in Fig. 4 in blue together with corresponding mechanical data; i.e. UTS (black) and TE data (red). Maximum and minimum values of the mechanical properties are shown as error bars to indicate the experimental scatter. The data for the reference material Fe–13.5Cr–0.45C is plotted in Fig. 4a, while the effects of alloying additions of Mn, Si and both Mn plus Si combined are shown in Fig. 4(b–d), respectively. For all four alloys the austenite content increases with temperature and exhibits a peak after tempering at 400 °C for 30 min. Both absolute values and their relative changes with temperature, however, show strong variations as a function of the respective alloying elements: adding Mn increases the respective austenite fractions compared to the equivalent reference material conditions, especially for the peak value (~factor 3). The ductility of the Fe–13.5Cr–0.45C–2.5Mn alloy follows the same trend as the austenite fraction, resulting in a similar strength as the reference material (UTS about 1500 MPa) but with a higher TE (18%). The austenite fractions of the Fe–13.5Cr–0.45C–2Si alloy are very similar to those of the reference material except for the peak value, which is more than four times larger. Nevertheless, no pronounced changes in ductility can be observed. The alloy Fe–13.5Cr–0.45C–2.5Mn–2Si exhibits the highest initial austenite content, but a much more gradual slope as the temperature for austenite reversion treatment increases, and a much lower peak value than the Mn and Si alloyed steels. Only a very modest correlation between austenite fraction and ductility as well as strength can be observed.

More details concerning the changes in austenite fraction, distribution and morphology of four selected alloys during tempering are shown in Fig. 5. The colour-coded EBSD phase maps (martensite: red, austenite: green) shown on the left hand side of the respective image pairs represent the as-quenched state; images on the right hand side correspond to the same alloys after quenching plus tempering at 400 °C for 30 min, respectively.

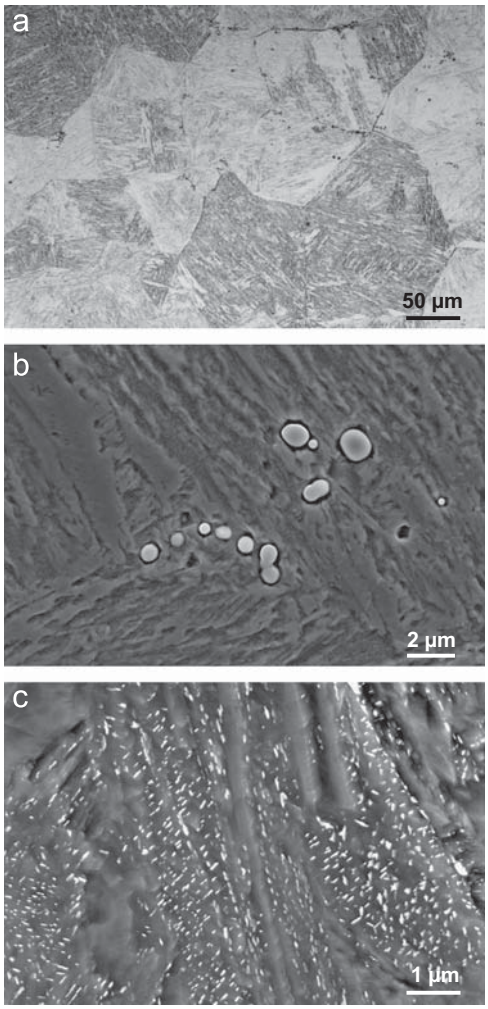

Fig. 3. Exemplary optical and scanning electron micrographs showing: (a) martensitic microstructure in the alloy 13.5Cr–0.45C (as quenched), (b) coarse carbides in the alloy 13.5Cr–0.45C–2.5Mn (as quenched), (c) fine platelets of nano-sized carbides in the alloy 13.5Cr–0.45C–2.5Mn after tempering at 400 °C for 30 min.

The image quality data is superimposed in grey scale; epsilon martensite is not taken into account due to its negligible volume fraction (maximum 2 vol%) and low confidence index. After quenching, 0.6 vol% retained austenite, with grain sizes ranging from about 5 down to 0.5 μm (scan resolution) was detected in the reference material (Fig. 5a). After tempering, the austenite fraction of the reference alloy increases to 11.6 vol% (reverted austenite), via growth of already existing (retained) austenite grains located at former austenite grain boundaries, as well as by the formation of new micro-sized austenite grains within the matrix. Addition of 2.5 wt% Mn (Fig. 5b) results in a slightly increased amount of retained austenite after quenching (3.2 vol%) and also in a larger retained austenite grain size (~10 μm), compared to the reference material. Tempering the 13.5Cr–0.45C–2.5Mn steel considerably increases the total amount of austenite to 35.4 vol%, both by more pronounced growth of the retained austenite grains and an increased formation of fine and more evenly dispersed austenite compared to the reference material. Adding 2 wt% Si (Fig. 5c) effectively suppresses retained austenite (0.2 vol% in the as-quenched state), but greatly promotes the formation of fine grained reverted austenite to a total amount of 48.4 vol% after tempering at 400 °C for 30 min. While the alloy Fe–13.5Cr–0.45C–2.5Mn–2Si (Fig. 5d) exhibits the largest amount of retained austenite of all alloys (5.9 vol% and up to 20 μm large grains), tempering results in less detectable austenite (25.1 vol%) than the materials containing only Mn or Si, respectively. The austenite reversion of the Mn–Si alloyed steel seems to proceed essentially via growth of the retained austenite grains and to a lesser extent by the formation of reverted austenite grains, which appear to form clusters along the former austenite grain boundaries.

Nano-indentation experiments (Fig. 6) were performed to obtain insight into the corresponding local mechanical properties of the different multiphase microstructures shown in Fig. 5. Colour-coded nano-hardness maps of the alloys containing 2.5 wt% Mn, 2 wt% Si and 2.5 wt% Mn plus 2 wt% Si, all after tempering at 400 °C for 30 min, are shown in Fig. 6(a–c), respectively. The nano-hardness distributions for the maps of Fig. 6(a–c) are plotted in Fig. 5d together with their respective colour code. The higher hardness values, compared to the corresponding macroscopic Rockwell data (Fig. 1d), are related to the much lower load of the nano-indentation setup. For the alloy Fe–13.5Cr–0.45C–2.5Mn a quasi-Gaussian coherent hardness distribution can be observed (Fig. 6a and d) with an average (peak) value of about 750 HV. Alloying additions of 2 wt% Si result in a similar distribution (Fig. 6b and d), only slightly shifted to a higher average value of about 810 HV. This increase in hardness correlates with the macroscopic observations (43.3 HRC for the Mn alloyed steel, 50.7 HRC for the Si alloyed material), despite the higher austenite fraction for the alloy Fe–13.5Cr–0.45C–2Si (48.4 compared to 35.4 vol%, Fig. 5b and c). In case of the combined addition of Mn and Si (Fig. 6c and d, macro-hardness 32.3 HRC), however, the nano-hardness values span a broader range and a more bimodal distribution can be observed: while large areas exhibit only about 600 HV, considerable fractions of the investigated cross section yield about 1000 HV and more.

5. Discussion

5.1. Rapid alloy prototyping of martensitic stainless steels

By utilising a novel bulk RAP approach [6], the effect of Mn and Si additions on microstructure and mechanical properties (Fig. 1) of martensitic stainless steels could be systematically investigated. The presented synthesis, processing and mechanical testing cycles for all six different alloys, including seven different heat treatments for each composition, was performed within ten days, so that chemistry- and TMT-related trends could be identified (Figs. 2–4). Those samples with the most interesting property profiles were selected for a more thorough microstructure characterisation using SEM and nano-indentation probing (Figs. 5 and 6). Special emphasis was placed on the formation of austenite as a function of chemical composition and tempering conditions, as well as on its effectiveness in improving martensite ductility (Fig. 4).

5.2. Influence of chemical composition on austenite formation

Two types of austenite could be detected in the quenched plus tempered alloys (Fig. 4), namely, retained and reverted austenite. For both types the relative fraction, grain size, morphology and dispersion is strongly linked to the respective alloying additions, as are the kinetics of martensite-to-austenite reversion (Fig. 5). For the reference alloy of this study (Fe–13.5Cr–0.45C), 0.6 vol% of retained austenite was detected. This finding is attributed to the high austenitisation temperature of 1150 °C. It is much higher than the austenitisation temperature used in typical heat treatments for tooling applications. The high temperature promotes the complete dissolution of the carbides and hence leads to a high solute C content, which in turn stabilises the austenite. For a 13.5 wt% Cr

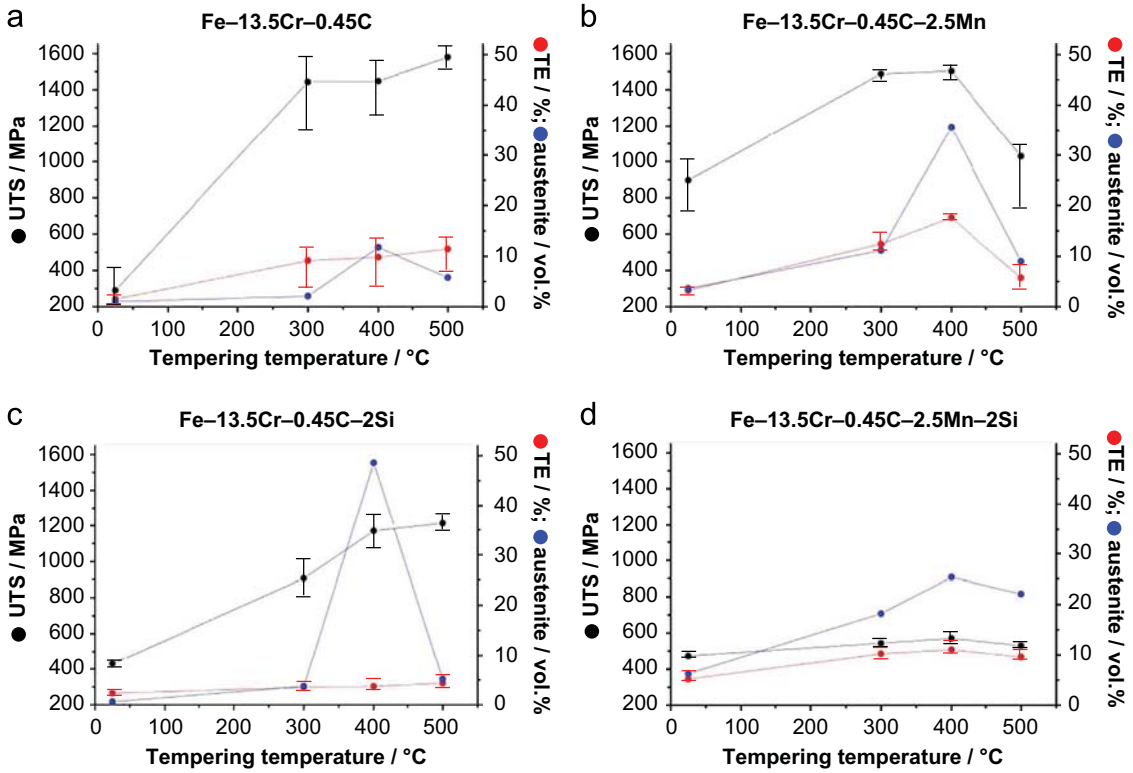

Fig. 4. Correlation between austenite fraction, ultimate tensile strength (UTS) and total elongation (TE) as function of tempering temperature (duration: 30 min) of four selected alloys. (For interpretation of the references to colour in this figure, the reader is referred to the web version of this article.)

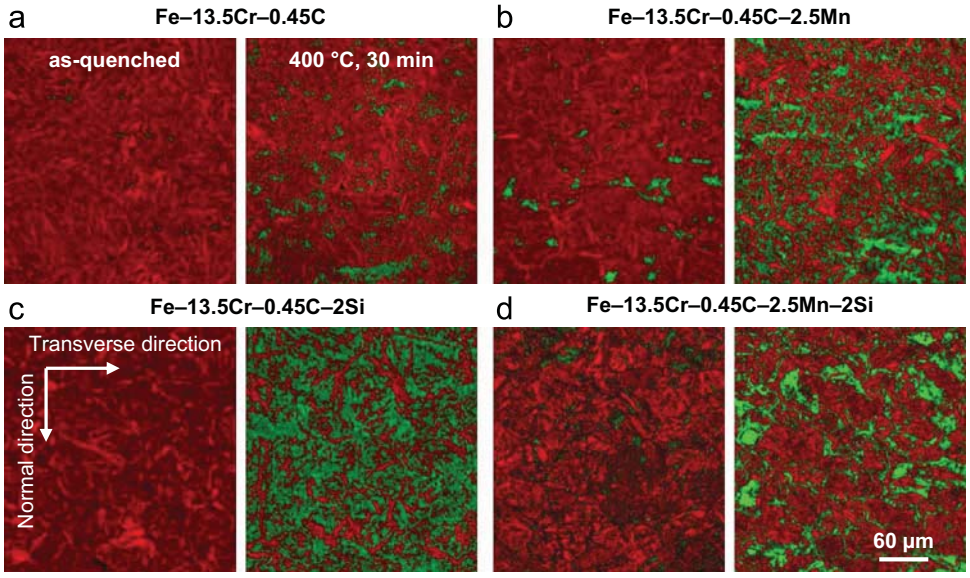

Fig. 5. Colour-coded EBSD phase maps (austenite: green; martensite: red) of four selected alloys in the as-quenched state (left images) and after tempering at 400 °C for 30 min (right images), respectively. The image quality data is superimposed in grey scale. (For interpretation of the references to colour in this figure legend, the reader is referred to the web version of this article.)

and 0.44 wt% C steel a M_S temperature of 118 °C was reported for similar experimental conditions [35]. While both, Mn and Si further decrease M_S according to the literature, Mn shows a much stronger effect [41,44,54]. Consequently, minor additions of Si left the retained austenite fraction virtually unaffected (0.2 vol% for the alloy Fe–13.5Cr–0.45C–2Si), while increasing Mn concentrations effectively stabilised the austenite, with 3.2 vol% for the 2.5-Mn alloy and up to 6.8 vol% for the material containing 5 wt% Mn (Figs. 4 and 5) in the as-quenched state. The local formation of retained austenite is further promoted by the tendency of Mn to segregate during steel synthesis and processing [55–59]. In this context it has to be noted that while the relatively large EBSD maps used in this study enable a sufficiently reliable statistical analysis, the correspondingly large step size used in the EBSD mapping (1 µm step size) limits the detection of grains with a size below this value. The amount of retained austenite of the alloy

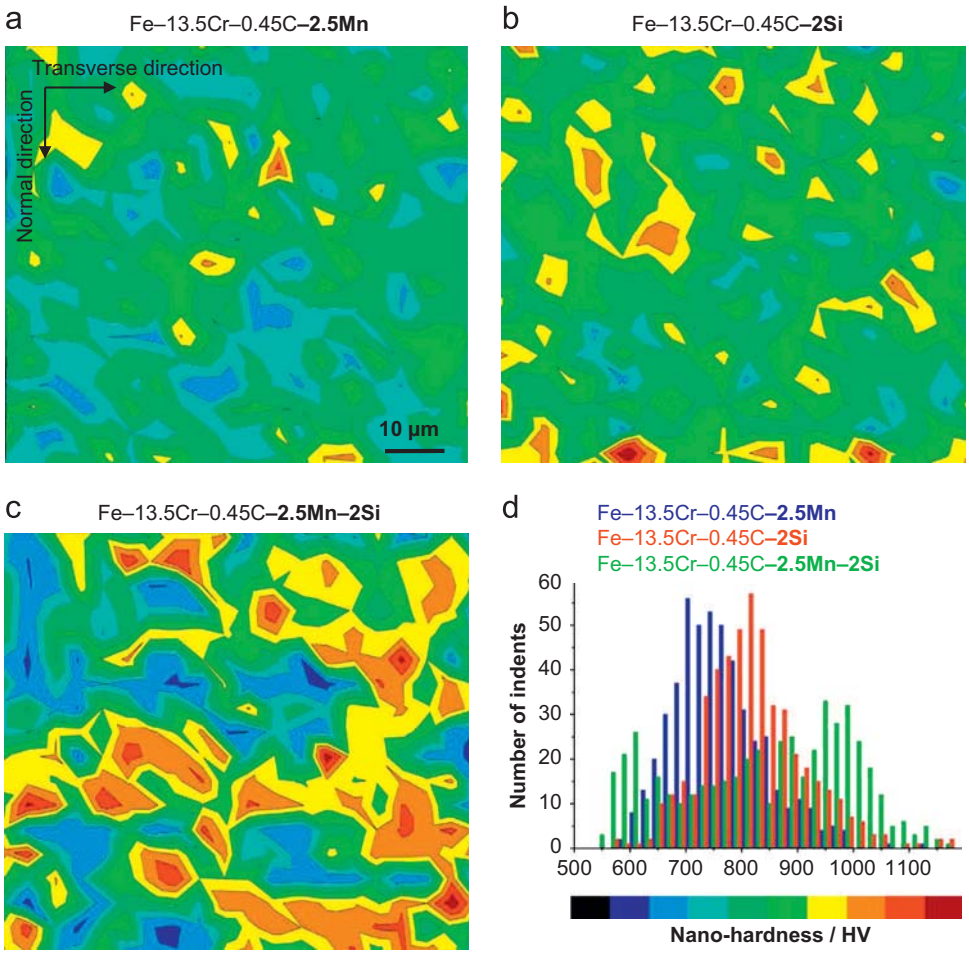

Fig. 6. Nano-indentation results of three selected alloys after tempering at 400 °C for 30 min: (a–c) colour coded nano-hardness maps; (d) corresponding nano-hardness distribution and colour-scale of the three maps. (For interpretation of the references to colour in this figure legend, the reader is referred to the web version of this article.)

containing both Mn and Si is with 5.9 vol% higher than the corresponding values observed for the alloys containing only either Si or Mn (Fig. 4). This non-linearity is expected in view of the reportedly complex and even equivocal role of Mn on austenite formation/retention in rapidly cooled steels [60–63].

According to Yuan et al. [35], austenite reversion during tempering of martensitic stainless steels is controlled by partitioning, segregation and kinetic freezing of C, as the mobility of substitutional elements such as Cr is too low at the chosen tempering temperatures [35]. Following this scenario, formation and growth of austenite can only occur if the C-concentration is high enough to provide a sufficient thermodynamic driving force during the martensite-reversion heat treatment, given the nucleation barrier is overcome. In the latter context it must be considered that the nucleation of austenite reversion in a martensite matrix is usually not only promoted by the segregation of elements that stabilise austenite (for instance on the lath grain boundaries) but also by the gain in elastic distortion energy that is released when the martensite is transformed into austenite [64–66]. The actual local C-concentration during quenching and subsequent reversion tempering is governed by two competing reactions [22,35]. These are the equilibrium segregation of C at martensite lattice defects, C-enrichment inside the retained austenite through equilibrium partitioning, and local C-depletion in the martensite via the formation of various carbides upon tempering (i.e. Fe_2C, M_3C, M_7C_3, $M_{23}C_6$ [34,42,67]). As a result, the amount of reverted austenite (i.e. total fraction minus retained austenite) follows a characteristic trend as a function of the tempering temperature, as observed in Fig. 6a, with a maximum value at 400 °C. Additionally, all three factors (required C-concentration, C-enrichment, carbide formation) also strongly depend on the materials' chemical composition, which can explain the different effects of Mn and Si additions [41,42] (Fig. 7a).

Of the factors governing the extent of austenite reversion, the required C-concentration to stabilise the fcc over the bcc lattice structure can be estimated by CALPHAD-predictions (Thermo-Calc version S, database SSOL2) as a function of tempering temperature. As can be seen in Fig. 7b, at the bulk C-concentration of 0.45 wt%, bcc is the stable phase for all alloys. The (locally) required C-concentration to reach equilibrium with fcc (critical concentration, Fig. 7b), systematically drops with temperature and characteristically varies with substitutional alloying (Fig. 7c). The addition of 2.5 wt% Mn effectively lowers the critical C-concentration by about 0.3 wt% compared to the reference alloy. This strong effect of Mn is in good agreement with matching observations of increased austenite reversion in the Mn-alloyed material (Figs. 5 and 7a). This is likely to be further enhanced by possible micro-segregations of Mn at martensite laths [41,46,55,57], which may also account for the occurrence of austenite clustering. Si, on the other hand, is thermodynamically not as effective in lowering the critical C-concentration, but in practice it strongly affects the formation of carbides in terms of type and temperature range, and in turn increases the activity of C [43–45]. The resultant austenite reversion of the alloy containing 2 wt% Si is much stronger and ubiquitous (almost 50 vol% after tempering at 400 °C for 30 min) but limited to a more narrow temperature range (Fig. 7a). Combined additions of 2.5 wt% Mn and 2 wt% Si give the lowest critical

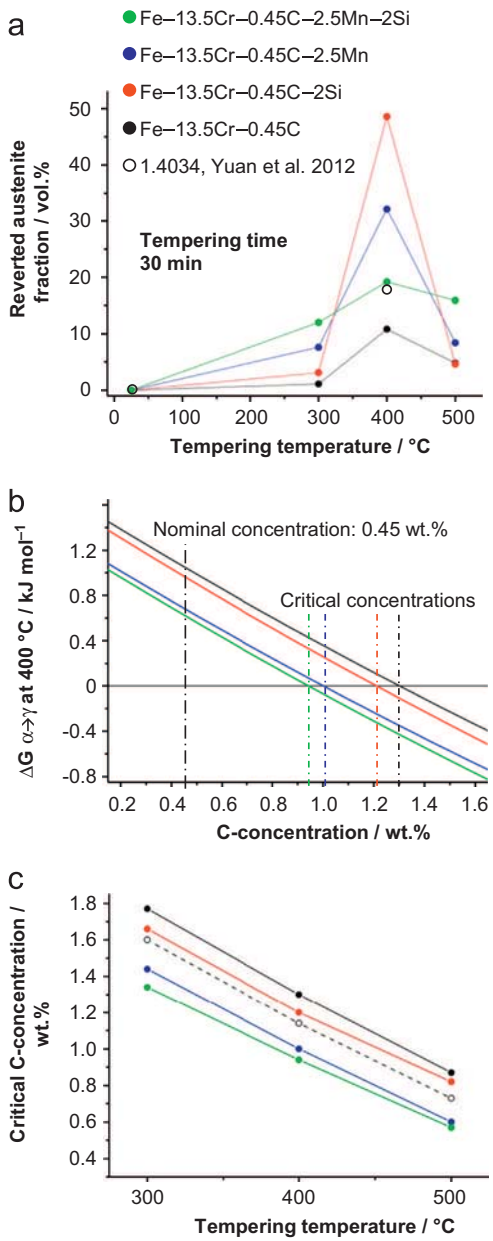

Fig. 7. Austenite reversion influenced by chemical composition, in comparison to literature data [35]: (a) reverted austenite fraction measured as function of tempering temperature; (b) CALPHAD-based determination of the critical carbon content required for austenite reversion; (c) critical carbon content as function of tempering temperature.

C-concentrations for austenite stability, which is supported by the microstructural observations of the alloy Fe–13.5Cr–0.45C–2.5Mn–2Si for tempering at 300 °C and 500 °C. The corresponding peak value at 400 °C, however, is much lower than for sole additions of Mn and Si. This finding, together with the austenite reversion appearing mainly as growth of the retained austenite grains rather than the formation of fine grains at martensite laths (Fig. 5c), clearly requires more detailed work. It is thereby a good example for future 'up-scaling' options, enabling the production and processing of large quantities of material by conventional metallurgical methods. Also it is a field for more detailed investigations using transmission electron microscopy or APT, guided by insights gained through a high-throughput RAP-screening, thus allowing for an efficient and knowledge based alloy design process.

Also included into Fig. 7a and c are calculations by Yuan et al. [35] for the industrially produced steel 1.4034 containing 13.5 wt% Cr and 0.44 wt% C. Despite the comparatively small amount of additional elements being present as impurities in this material (0.53Mn, 0.28Si, 0.16Ni, 0.02N; all in wt% [35]), the retained and reverted austenite fractions are significantly increased and the critical C concentration reduced in comparison to the reference alloy of this study. This highlights the complexity and interdependence of alloying elements on austenite retention and reversion phenomena.

5.3. *Influence of retained and reverted austenite on the mechanical properties*

Austenite is the only microstructure constituent of the investigated steels to undergo appreciable plastic deformation and lend ductility to the strong martensitic matrix. Hence, as the fraction of (retained) austenite is increased by adding Mn to the reference state, the ductility – and thus usable strength – of the steels in the as-quenched state becomes higher (Fig. 1).

Tempering, as discussed in the previous section, generates additional reverted austenite, but no straightforward link between the austenite fraction and the respective materials strength and ductility could be observed in the investigated alloys (Fig. 4). Apparently, the extremely differing material properties as function of chemical composition (exemplified in Fig. 2) are the result of not only the austenite volume fraction, but also its respective grain size (dispersion), distribution, and stability (Fig. 5). Of specific interest in this context is the range of the austenite stability against martensitic transformation upon mechanical loading [18,19,37]. Here the mechanical mapping results of the nano-indentation experiments (Fig. 6) and the phase maps (Fig. 5) provide some insight: only a favourable combination of all those factors leads to the desired simultaneous achievement of both strength and ductility. In case of the reference alloy, the comparatively little amount of small to medium sized reverted austenite grains (Fig. 5a) and their reasonable dispersion enables to effectively exploit the materials' high strength of almost 1600 MPa (the maximum UTS value of all investigated alloys). Mn additions lead to well dispersed, very fine grained reverted austenite in addition to small amounts of medium sized retained (and subsequently grown) austenite. The resulting range of austenite stability and ductility is probed qualitatively by the EBSD image quality (shown jointly with phase map Fig. 5b) and the nano-hardness (Fig.6a), respectively: the lower EBSD image quality of the newly formed reverted austenite indicates a larger dislocation density compared to the retained austenite [68]. The variety in dislocation content and size [26,32,69] translates to a corresponding variety in the critical strains for martensitic transformation. Such microstructure heterogeneity promotes an integral mechanical response that is characterised by gradually stimulated and hence, more permanent strain-hardening as shown by the blue curve in Fig. 2. The alloy containing 2.5 wt% Mn hence reveals the most attractive combination of mechanical properties of all the investigated steels by the utilisation of this gradually activated and heterogeneous TRIP effect [18,35].

Si additions, on the other hand, led to massive formation of interconnected, fine grained reverted austenite (Fig. 5c), but the materials remained hard (Fig. 6b) and brittle. It seems that the Si-induced reverted austenite is either so stable that it does not transform to martensite during deformation, or that it transforms simultaneously at low elongations to brittle martensite containing high amounts of C (large critical C-concentration, Fig. 7b). Austenite stabilisation may result from C-supersaturation [45], austenite morphology [37,70] or the hydrostatic pressure of the surrounding martensite [71,72].

The drastically lowered YS and still limited ductility of the alloy containing both Mn and Si seems to be the result of its disadvantageous, bimodal microstructure, which consists of a network of large and instable austenite grains embedded in a hard martensitic matrix containing almost no fine-grained, newly formed austenite (Figs. 5d and 6c) [70,72].

It should be emphasised that the results of this study were obtained using the RAP approach, and that consequently some specific effects of this efficient high-throughput screening procedure need to be taken into account [6]. This means that conventional processing might provide slightly different mechanical and microstructure results. This applies particularly for the streamlined TMT setup (coarse grained microstructure due to homogenisation and austenitisation in one step), tensile testing procedure (decreased ductility of high-throughput flat sheet specimens with remaining scales and surface roughness from processing) and phase identification experiments (only EBSD measurements, large maps with good statistics but limited resolution). These factors, together with the already discussed deviations in chemical composition, may explain the differences compared to the data reported by Yuan et al. [35] in terms of the respective austenite contents (see previous section) and mechanical properties of 1.75 GPa UTS and 23% elongation.

6. Summary and conclusions

This study applies a novel bulk high throughput synthesis, processing and tensile testing sequence with the goal of identifying ductile martensitic compositions and optimal microstructures. Regarding the composition the effects of both, single and combined alloying additions of Mn (0–5 wt%) and Si (0–2 wt%) on the microstructure and mechanical properties of a group of 13.5Cr–0.45C (wt%) based martensitic stainless steels were examined. Tensile and hardness testing was performed on a matrix of six alloys and seven tempering conditions (300, 400 and 500 °C for 0, 10 and 30 min each) following the recently introduced rapid alloy prototyping approach. Based on the results obtained from this high throughput bulk combinatorial screening, special emphasis was placed on austenite reversion phenomena and their potential to enhance martensite ductility while conserving strength as a function of the chemical composition of the investigated steels. The following conclusions can be drawn:

(1) Mn additions increase the fraction of austenite retained after quenching from 1150 °C and thereby improve the ductility and usable strength of the martensitic matrix. Upon tempering at 400 °C for 30 min, the best combination of strength and ductility (about 1.5 GPa UTS and 18% tensile elongation) is observed for the alloy containing 2.5 wt% Mn. Si additions lead to the highest hardness but also the most brittle material behaviour, almost unaffected by tempering. Combined additions of 2.5 wt% Mn and 2 wt% Si result in low hardness and very low YS values (400 MPa), but nevertheless a maximum elongation of only 12%.
(2) All investigated alloys exhibit austenite reversion during tempering, which peaks at 400 °C. The respective absolute and temperature dependencies, however, greatly change with the chemical composition of the steels. Mn and Si appear to effectively influence the three partly competing factors for the mainly C-controlled austenite reversion; i.e. the required C-concentration for a sufficient thermodynamic driving force, the locally achievable C-enrichment via partitioning and segregation at local defects, and the formation of carbides.
(3) The differing properties of the materials were observed to be caused not only by the differences in austenite fraction, but also by its grain size, dispersion and in turn stability against martensitic transformation. Mn additions apparently impart optimum mechanical properties via a large number of fine austenite grains with a variety of critical strains. Si leads to high contents of austenite (up to 50 vol%) but of either too high stability or non-favourable transformation behaviour. Large amounts of Mn and Si together form a bimodal microstructure of large, net-like distributed austenite grains which is believed transform easily and rapidly, thereby not promoting ductility.
(4) While its potential of enhancing martensite ductility was clearly demonstrated, additional work is required to gain more insight into the mechanisms of austenite reversion as a function of chemical composition as well as its respective transformation behaviour during deformation. Especially the role of carbide formation, or the effect of other alloying elements such as nitrogen, need to be investigated using higher resolution characterisation techniques such as TEM and APT.
(5) The RAP approach has been successfully applied to rapidly investigate the chosen matrix of alloy systems and tempering conditions, as well as to identify the corresponding microstructural trends and their relation to the mechanical properties. This allows for efficient and knowledge based alloy design, as the aforementioned issues can now be readily addressed in a mechanism-targeted and efficient 'up-scaling' based on the insights gathered from this high throughput screening using conventional metallurgical, processing and testing methods.

Acknowledgements

C. Baron is acknowledged for support with mechanical testing, J. Wang for providing data obtained during her master thesis work.

References

[1] A.K. Gupta, D.R. Kumar, J. Mater. Process. Technol. 172 (2006) 225–237.
[2] O. Bouaziza, S. Allaina, C.P. Scotta, P. Cugya, D. Barbier, Curr. Opin. Solid State Mater. Sci. 15 (2011) 141–168.
[3] I. Gutierrez-Urrutia, J.A. del Valle, S. Zaefferer, D. Raabe, J. Mater. Sci. 45 (2010) 6604–6610.
[4] I. Gutierrez-Urrutia, D. Raabe, Acta Mater. 59 (2011) 6449–6462.
[5] D.R. Steinmetz, T. Jäpel, B. Wietbrock, P. Eisenlohr, I. Gutierrez-Urrutia, A. Saeed–Akbaric, T. Hickel, F. Roters, D. Raabe, Acta Mater. 61 (2013) 494–510.
[6] H. Springer, D. Raabe, Acta Mater. 60 (2012) 4950–4959.
[7] I. Gutierrez-Urrutia, D. Raabe, Acta Mater. 60 (2012) 5791–5802.
[8] G. Frommeyer, U. Brüx, Steel Res. Int. 77 (2006) 627–633.
[9] K.M. Chang, C.G. Chao, T.F. Liu, Scr. Mater. 63 (2010) 162–165.
[10] W.K. Choo, J.H. Kim, J.C. Yoon, Acta Mater. 45 (1997) 4877–4885.
[11] Y.J. Li, P. Choi, S. Goto, C. Borchers, D. Raabe, R. Kirchheim, Acta Mater. 60 (2012) 4005–4016.
[12] D. Raabe, et al., MRS Bull. 35 (2010) 982.
[13] Y.J. Li, P. Choi, C. Borchers, S. Westerkamp, S. Goto, D. Raabe, R. Kirchheim, Acta Mater. 59 (2011) 3965–3977.
[14] Y.I. Son, K.L. Young, K.T. Park, C.S. Lee, D.H. Shin, Acta Mater. 53 (2005) 3125–3134.
[15] M. Calcagnotto, D. Ponge, D. Raabe, Mater. Sci. Eng. A 527 (2010) 7832–7840.
[16] G.B. Olson, M. Cohen, J. Less Common Met. 28 (1972) 107–118.
[17] G.B. Olson, M. Azrin, Metall. Trans. A 9A (1978) 713–721.
[18] J. Wang, S. van der Zwaag, Metall. Mater. Trans. A 32A (2001) 1527–1539.
[19] M.Y. Sherif, Mater. Sci. Technol. 20 (2004) 319.
[20] J.G. Krauss, M. Cohen, Trans. Am. Inst. Metall. Eng. 224 (1962) 1212.
[21] J.F. Breedis, Trans. Am. Inst. Eng. 236 (1966) 218.
[22] O. Dmitrieva, D. Ponge, G. Inden, J. Millán, P. Choi, J. Sietsma, D. Raabe, Acta Mater. 59 (2011) 364–374.
[23] Y.K. Lee, H.C. Shin, D.S. Leem, J.Y. Choi, W. Jin, C.S. Choi, Mater. Sci. Technol. 19 (2003) 393.
[24] R Montaneri, Z. Metallk. 81-H2 (1990) 114.
[25] Y. Ma, J.-E. Jin, Y.-K. Lee, Scr. Mater. 52 (2005) 1311.
[26] S. Rajasekhara, L.P. Karjalainen, A. Kyröläinen, P.J. Ferreira, Mater. Sci. Eng. A 527 (2010) 1986–1996.

[27] G. Krauss, Acta Metall. 11 (1963) 499.
[28] S. Jana, C.M. Wayman, Trans. Am. Inst. Eng. 239 (1967) 1187.
[29] H. Kessler, W. Pitsch, Acta Metall. 15 (1967) 401.
[30] K.B. Guy, E.P. Butler, D.R.F. West Met, Science 17 (1983) 167–176.
[31] K. Tomimura, S. Takaki, Y. Tokunuga, ISIJ Int. 31 (1991) 1431–1437.
[32] O. Thuillier, F. Danoix, M. Gouné, D. Blavette, Scr. Mater. 55 (2006) 1071.
[33] J. Speer, D.K. Matlock, B.C De Cooman, J.G. Schroth, Acta Mater. 51 (2003) 2611–2622.
[34] D.V. Edmonds, K. He, F.C. Rizzo, B.C. De Cooman, D.K. Matlock, J.G. Speer, Mater. Sci. Eng. A 25 (2006) 438–440.
[35] L. Yuan, D. Ponge, J. Wittig, P. Choi, J.A. Jiménez, D. Raabe, Acta Mater. 60 (2012) 2790–2804.
[36] N. Nakada, T. Tsuchiyama, S. Takaki, N. Miyano, ISIJ Int. 51 (2011) 299–304.
[37] A.S. Podder, I. Lonardelli, A. Molinari, H.D.H. Bhadeshia, Proc. R. Soc. A 467 (2011) 3141.
[38] J.W. Morris, Z. Guo, C.R. Krenn, Y.H. Kim, ISIJ Int. 41 (2011) 599.
[39] D. Zou, Y. Han, W. Zhang, X. Fang, J. Iron Steel Res. Int. 17 (2010) 17.
[40] H. Smith, D.R.F. West, J. Mater. Sci. 8 (1973) 1413.
[41] E. De Moor, D.K. Matlock, J.G. Speer, M.J. Merwin, Scr. Mater. 64 (2011) 185–188.
[42] D. Edmonds, D. Matlock, J. Speer, La Metall. Ital. 1 (2011) 41–48.
[43] R. Bernst, G. Inden, A. Schneider, Comput. Coup. Phase Dia. Thermochem. 32 (2008) 207–216.
[44] S.S. Nayaka, R. Anumolu, R.D.K. Misra, K.H. Kimc, D.L. Lee, Mater. Sci. Eng. A 498 (2008) 442–456.
[45] B.C. De Cooman, Mater. Sci. 8 (2004) 285–303.
[46] J. Lis, J. Morgiel, A. Lis, Mater. Chem. Phys. 81 (2003) 466–468.
[47] S.S. Babu, K. Hono, T. Sakurai, Appl. Surf. Sci. 67 (1993) 321–327.
[48] Y. Takahama, M.J. Santofimia, M.G. Mecozzi, L. Zhao, J. Sietsma, Acta Mater. 60 (2012) 2916–2926.
[49] M.G. Michal, F. Ernst, A.H. Heuer, Metall. Mater. Trans. A 37 (2006) 1819.
[50] T. Gebhardt, D. Music, M. Ekholm, I.A. Abrikosov, L. Vitos, A. Dick, T. Hickel, J. Neugebauer, J.M. Schneider, J. Phys.: Condens. Matter 23 (2011) 246003.
[51] J. Cui, Y.S. Chu, O.O. Famodu, Y. Furuya, J. Hattrick-Simpers, R.D. James, A. Ludwig, S. Thienhaus, M. Wuttig, Z. Zhang, I. Takeuchi, Nat Mater. 5 (2006) 286–290.
[52] X. Zheng, D.G. Cahill, J.C. Zhao, Acta Mater. 58 (2011) 1236–1241.
[53] J.C. Zhao, X. Zheng, D.G. Cahill, JOM 63 (2011) 40.
[54] G. Krauss Steels, Processing, Structure and Performance, ASM International, Materials Park, Ohio, USA, 2005.
[55] D. Senk, H. Emmerich, J. Rezende, R. Siquieri, Adv. Eng. Mater. 9 (2007) 695.
[56] T.F. Majka, D.K. Matlock, G. Krauss., Metall. Mater. Trans. A 33 (2002) 1627.
[57] S.H. Mun, M. Watanabe, X. Li, K. Oh, D.B. Williams, H.C. Lee, Metall. Mater. Trans. A 33 (2002) 1057.
[58] E.A. Wilson, Metall. Mater. Trans. A 35 (2004) 352.
[59] M. Nasim, B.C. Edwards, E.A. Wilson, Mater. Sci. Eng. A 281 (2000) 56–67.
[60] A.L. Schaeffler, The Iron Age72.
[61] N. Suutula, Metall. Trans. A 13 (1982) 2121.
[62] S.R. Chen, H.A Davies, W.M. Rainforth, Acta Mater. 47 (1999) 4555–4569.
[63] F.C. Hull, Weld. Res. J. (52) (1973) 193.
[64] S. Rajasekhara, P.J. Ferreira, Acta Mater. 59 (2011) 738–748.
[65] N. Nakada, T. Tsuchiyama, S. Takaki, S. Hashizume, ISIJ Int. 47 (2007) 1527–1532.
[66] P.C. Clemm, J.C. Fisher., Acta Metall. 3 (1955) 70.
[67] L.S. Malinov, A.P. Cheilyakh, O.D. Cheilyakh, Metalloved. Term. Obrab. Met. 8 (1988) 12–15.
[68] V.G. Gorbach, I.V. Sidoruk, E.A. Izmailov, Metalloved. Term. Obrab. Met. 8 (1988) 9–12.
[69] M.C. Somani, P. Juntunen, L.P. Karjalainen, R.D.K Misra, A. Kyröläinen, Metall. Mater. Trans. A 40 (2009) 729.
[70] E. Jimenez-Melero, N.H. van Dijk, L. Zhao, J. Sietsma, S.E. Offerman, J.P. Wright, S. van der Zwaag, Acta Mater. 55 (2007) 6713–6723.
[71] H. Berns, W. Theisen, Eisenwerkstoffe Stahl und Gusseisen, Springer Verlag, Berlin, Heidelberg, 2006.
[72] D.Q. Bai, A.D. Chiro, S. Yue, Mater. Sci. Forum 284 (1998) 253–262.